

Single-Molecule Tribology: Force Microscopy Manipulation of a Porphyrin Derivative on a Copper Surface

Rémy Pawlak,^{*,†} Wengen Ouyang,[‡] Alexander E. Filippov,[§] Lena Kalikhman-Razvozov,^{||} Shigeki Kawai,[†] Thilo Glatzel,[†] Enrico Gnecco,[¶] Alexis Baratoff,[†] Quanshui Zheng,[‡] Oded Hod,^{||} Michael Urbakh,^{*,||} and Ernst Meyer^{*,†}

[†]Department of Physics, University of Basel, Klingelbergstrasse 82, Basel 4056, Switzerland

[‡]Center for Nano and Micro Mechanics, Tsinghua University, Beijing 100084, China

[§]Donetsk Institute for Physics and Engineering, National Academy of Sciences of Ukraine, Donetsk 83114, Ukraine

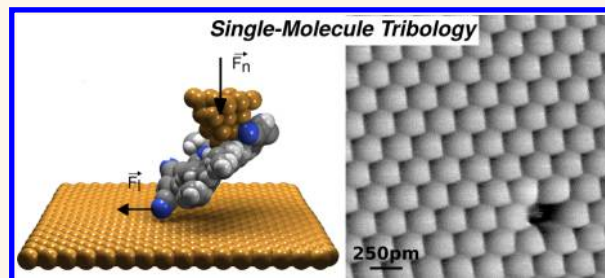
^{||}Department of Physical Chemistry, School of Chemistry, The Raymond and Beverly Sackler Faculty of Exact Sciences, and The Sackler Center for Computational Molecular and Materials Science, Tel Aviv University, Tel Aviv 6997801, Israel

[¶]Otto Schott Institute of Materials Research (OSIM), Friedrich Schiller University Jena, Jena 07743, Germany

Supporting Information

ABSTRACT: The low-temperature mechanical response of a single porphyrin molecule attached to the apex of an atomic force microscope (AFM) tip during vertical and lateral manipulations is studied. We find that approach–retraction cycles as well as surface scanning with the terminated tip result in atomic-scale friction patterns induced by the internal reorientations of the molecule. With a joint experimental and computational effort, we identify the dicyanophenyl side groups of the molecule interacting with the surface as the dominant factor determining the observed frictional behavior. To this end, we developed a generalized Prandtl–Tomlinson model parametrized using density functional theory calculations that includes the internal degrees of freedom of the side group with respect to the core and its interactions with the underlying surface. We demonstrate that the friction pattern results from the variations of the bond length and bond angles between the dicyanophenyl side group and the porphyrin backbone as well as those of the CN group facing the surface during the lateral and vertical motion of the AFM tip.

KEYWORDS: friction, nanotribology, atomic force microscopy, tip termination, porphyrin, Cu(111), Prandtl–Tomlinson, density functional theory



The design of molecular machines capable of directional motion on a surface constitutes nowadays an active field of scientific research.^{1,2} With this prospect, a detailed understanding of the internal degrees of freedom of single molecules is required to foresee their preferential dynamics and frictional behavior when confined to two-dimensional motion. Experimental studies aiming to gain such understanding must thus be performed with submolecular resolution in order to reveal the interplay between chemical composition and mechanical response. During the last two decades, the field of nanotribology provided valuable information to this end *via* nanoscale frictional measurements using atomic force microscopy (AFM) techniques.³ Here, the frictional force can be measured using a sharp AFM tip sliding across an atomically flat surface,^{4–9} resulting in atomic-scale friction patterns on various crystals^{10–14} as well as the

preferential displacements of nanometer-sized particles.^{15–17} Such experiments thus provide fundamental insights into the origins of friction at the nanoscale.^{4,7}

An important aspect in nanotribology concerns the tip–sample chemistry. To address this issue, several studies have been conducted by either scanning surfaces covered with self-assembled molecular layers^{18–21} or, alternatively, covering the AFM tip with few such layers, a technique often termed chemical force microscopy.^{22–24} With both approaches, however, understanding the fundamental origin of friction phenomena at the single-molecular level is a highly challenging task²⁵ since the number of molecules interacting with the tip

Received: September 13, 2015

Accepted: November 16, 2015

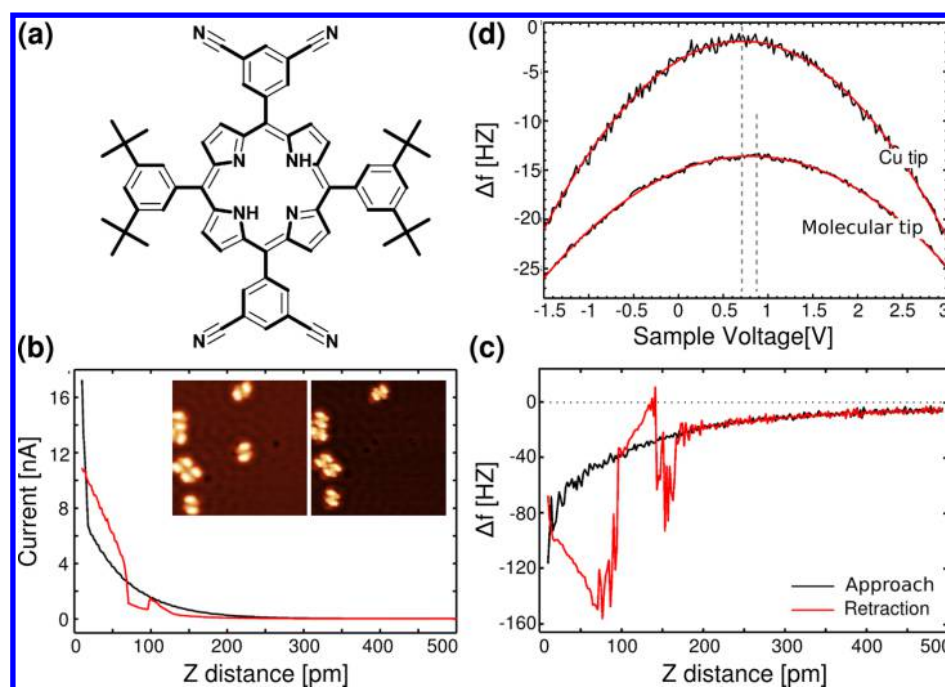


Figure 1. Chemical termination of the AFM tip apex. (a) Schematic of the free-base porphyrin functionalized with two meso-(3,5-dicyanophenyl) and two meso-(3,5-di-*tert*-butylphenyl). (b,c) Typical current (I) and frequency shift (Δf) variations as a function of tip–surface distance (Z) recorded during the functionalization of the tip apex at a tip–surface bias voltage of 1 mV. A background subtraction of 20 Hz was applied in panel c. (d) Comparison of $\Delta f(V)$ curves obtained with and without the tip termination. A modification of ≈ 200 mV of the local contact potential difference is observed after the tip termination. The inset of panel b shows a successful tip decoration, where a single molecule disappears from the STM image after being picked up by the tip, inducing a change of the STM contrast.

and their instantaneous conformations during the sliding process are usually uncontrolled. Thus, the apex termination remains unknown in term of its structure and chemical nature, a fact that severely restricts the final interpretation of the data. Recently, experimental strategies to intentionally pick up single molecules adsorbed on surfaces at the apex of local probes have been introduced at low temperature, leading to the systematic enhancement of imaging contrasts in scanning tunneling microscopy (STM), AFM, and Kelvin probe force microscopy (KPFM) experiments.^{26,27} Using this approach with relatively large molecules, new insights into the molecule–surface interactions^{28–30} and the mechanical properties of single molecules^{31–39} have become accessible.

In this work, we follow this approach and terminate the apex of a tuning fork sensor with a porphyrin derivative to study the intrinsic degrees of freedom of the molecule during vertical and lateral manipulations over a flat Cu(111) surface. Constant-height frequency shift $\Delta f(x,y)$ maps systematically reveal atomic-scale frictional patterns arising from the interaction of a single carbonitrile end group (CN) of the molecule with the surface potential. The measured frictional features turn out to be related to the mechanical response of the molecular structure acting as a spring between the tip apex and the underlying surface. Numerical simulations based on an extended Tomlinson model, parametrized *via* density functional theory (DFT), reveal that the variations of bond length and dihedral angle of a dicyanophenyl side group with respect to the porphyrin core as well as those of the CN group facing the surface play a crucial role in the frictional processes during both vertical and lateral manipulations.

RESULTS AND DISCUSSION

Tip Decoration. We decorate the AFM tip with a single free-base porphyrin core functionalized by two meso-(3,5-dicyanophenyl) and two meso-(3,5-di-*tert*-butylphenyl) peripheral rings (see Figure 1a).⁴⁰ Adsorbed on Cu(111), the porphyrin adopts a saddle conformation.³⁵ The tip apex is decorated by picking up one single porphyrin molecule from the Cu(111) surface by indenting the tip onto the center of the molecule and retracting it as discussed below (see inset of Figure 1b).

The tunneling current, $I(Z)$, and the frequency shift, $\Delta f(Z)$, simultaneously recorded as a function of tip–surface distance, z , during the functionalization process are shown in Figure 1b,c, respectively. An abrupt increase of the conductance during the approach is observed at a tip–surface distance of 20 pm (Figure 1b) accompanied by an increase (toward negative values) of the tuning fork frequency shift (Figure 1c). These indicate the attachment of the molecule to the tip, a process that is probably governed by specific chemical interactions between the functionalized porphyrin CN end groups and the copper-terminated apex at $Z = 20$ pm (Figure 1b).³⁵ While the tip is retracted, both the $I(z)$ and $\Delta f(z)$ channels reveal abrupt variations in a range of 0–200 pm as a consequence of a step-by-step detachment of the molecule from the surface.^{38,41} The total normal force extracted from these data is ≈ 6 –8 nN and can be associated with the force required by the tip to detach the molecule from the copper surface. Thereafter, the tip decoration can be confirmed by STM imaging, showing the disappearance of the molecule and a clear modification of the STM contrast. This can be further validated by measuring the variations of the tip’s local contact potential upon decoration. Figure 1d shows two $\Delta f(V)$ curves recorded before and after

the tip decoration above the Cu surface. The local contact potential difference (LCPD) above Cu(111) with a bare Cu tip is not zero due to the tip shape influence (≈ 700 mV). By comparing the curves, we observed a positive shift of the LCPD (≈ 150 – 200 mV) upon tip decoration that we attribute to the molecular tip termination.

Approach–Retraction Measurements. In order to gain better understanding of the tip–molecule junction structure, we measured the mechanical response of the system upon approach to and retraction from the copper surface. Figure 2a shows the typical dependence of the frequency shift on the

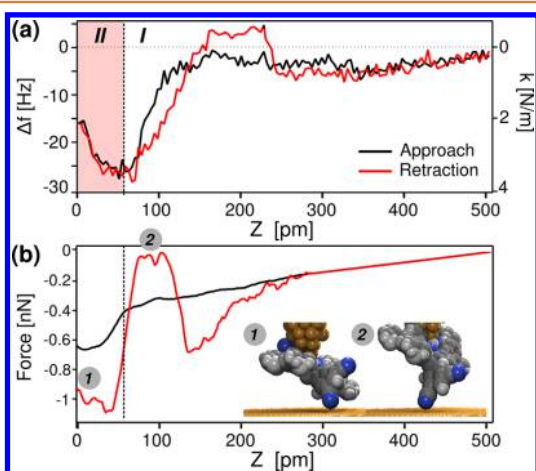


Figure 2. Molecular response during approach–retract tip manipulation. (a) Approach–retract $\Delta f(z)$ and $k_{ts}(z)$ curves obtained with a porphyrin attached to the tip. The van der Waals background (~ 19 Hz) induced by the chemical termination of the apex with the molecule has been subtracted. (b) Extracted normal force F_z . The inset shows an illustration of a possible sudden conformational change occurring during the retraction trace.

tip–surface distance, $\Delta f(z)$, after the removal of the van der Waals background (≈ 19 Hz in Figure 2) and the corresponding stiffness variations, $k_{ts}(z)$, obtained with a porphyrin attached to the tip. Compared to a bare metallic tip (Figure 1c), the approach curve shows characteristic differences. First, Δf and k_{ts} remain constant across an extended region of the tip–sample distance z (region I), followed by a steep decrease toward more negative values (region II) and a less steep increase toward positive values. The lower turning point of the $\Delta f(z)$ curve is always observable with decorated tips, whereas its observation is extremely rare in the case of bare copper tips.^{42,44} The retraction $\Delta f(z)$ curve (solid red line) shows a small hysteresis compared to the approach curve that we attribute to the mechanical response of the decorated tip during the stretching process, as reported in recent experiments.^{38,39} Therefore, we may relate the retraction $\Delta f(z)$ deviations from the non-terminated tip traces to the elasticity of the single-molecule junction formed between the tip and the surface.

This is best demonstrated when plotting (Figure 2b) the dependence of the normal force (extracted *via* simple integration of the measured data) on the tip–surface distance. As expected, at large distances, approaching the decorated tip to the surface results in a monotonic increase of the attractive force. Noticeably, at $Z \sim 60$ pm, an abrupt increase of the attractive force is observed that can be interpreted as a sudden conformational change of the molecule. Further approach to the surface results in a force plateau followed by a slight

decrease of the attractive interaction at very short distances due to steric repulsion. Upon retraction, a strong hysteresis is found with respect to the approach curve. Here, similar to the approach trace, at small distances, minor variations of the normal force are measured. Nevertheless, at 60 pm, a considerably sharper reduction of the measured force is observed, which can be attributed to a different conformational change of the molecule compared to the approach process (see inset of Figure 2b). This is followed by another strengthening of the attraction at ~ 130 pm that may correspond to a jump out of contact accompanied by a secondary conformational change. Similar instabilities have been previously observed by Wagner *et al.*³⁹ and interpreted as a consequence of the mechanics of the single-molecule junction. Our simulations of approach and retraction curves support this interpretation (see computational section below). At larger distances, the approach and retraction normal force curves collapse. We note that the deviation between the extracted approach and retraction forces at the shortest tip–surface distance may be attributed to the experimental noise and observed instabilities that affect the numerical quadrature cumulative sum.

Friction Measurements. The friction experiments have been conducted by approaching the porphyrin-terminated tip to the Cu surface while oscillating the tuning fork sensor at its resonance frequency with oscillation amplitudes $A_0 \approx 50$ pm. It is worth mentioning that an essential prerequisite to obtain the friction response presented below is the use of small oscillation amplitudes (below 50 pm), which avoids stochastic detachments of the molecule from the tip or the surface during its lateral motion. In this way, the experimental friction traces are only related to the mechanical response of the molecular structure between the tip and the surface. No significant tunneling current was detected during the approach, and the whole experiment was performed at zero bias. The formation of a local junction between the molecule and the surface, as illustrated in Figure 3a, was experimentally confirmed by a decrease of the frequency shift of ~ 10 Hz compared to larger tip–sample distances, in agreement with Figure 1c. Figure 3b shows a typical $\Delta f(x,y)$ map obtained by scanning the Cu(111) surface at constant height. The atomic-scale contrast observed in the image resembles the frictional patterns obtained by conventional frictional force microscopy on Cu(111).^{10,11} The vacancy defect indicated by the black arrow further indicates that atomic resolution is achieved. Note also that the contrast differs considerably from the atomic resolution conventionally obtained by noncontact atomic force microscopy (nc-AFM) on Cu(111),⁴² such that the fundamental motif appears to be diamond-shaped rather than round-shaped. The hexagonal surface lattice structure is, however, preserved and has a periodicity of ~ 0.25 nm, in relative good agreement with the Cu(111) surface lattice vector length of ~ 0.22 nm.⁴³ We note that during the constant-height imaging the molecule-terminated tip probes the surface at short-range distances where a stable molecule–surface junction is formed (region II in Figure 2a). In this regime, the normal force varies from -0.6 to -0.4 nN.

Figure 3c shows profiles of the tip–sample stiffness $k_{ts}(x)$ directly extracted from the $\Delta f(x,y)$ map. The normal force gradient $k_{ts} = -2k\Delta f/f$ varies from -2 to $+3$ N/m. The stiffness variation Δk_{ts} is ≈ 5 N/m, which corresponds to the tip–surface stiffness mediated by the porphyrin molecule. Importantly and despite the complex molecular structure attached to the tip, stable and nonstochastic atomic-scale sawtooth-like patterns are

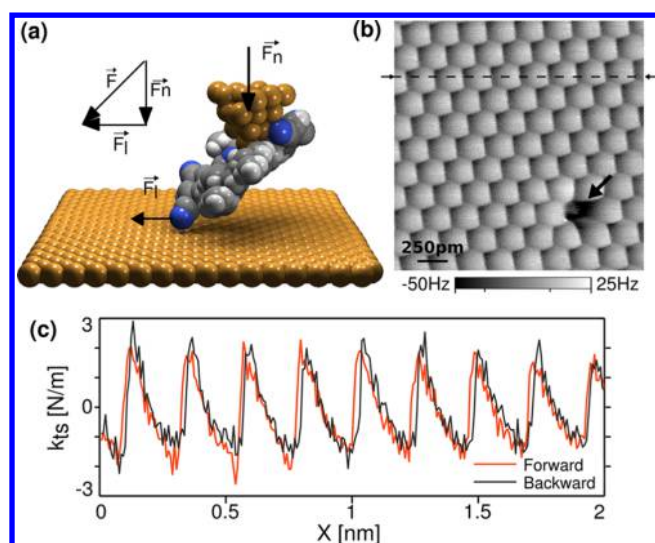


Figure 3. Mechanical response during lateral displacement. (a) Illustration of the friction experiment: the porphyrin-terminated tip is brought into contact with the Cu(111) surface while oscillating at its resonance frequency. (b) Constant-height $\Delta f(x,y)$ maps of the surface showing the atomic lattice structure of Cu(111). (c) Tip-sample stiffness k_{ts} profile taken along the straight trajectory marked by the dashed black line in panel b. The black arrow in panel b marks a possible lattice vacancy site.

systematically obtained, indicating the formation of a well-defined tip-sample junction during the experiment. The ability of the CN molecular end groups to coordinate with copper atoms of both the tip and the surface suggests that they play a major role in the formation of the single-point contact with the copper surface.³⁵

To investigate the interplay between tip-sample distance and frictional response, we suddenly reduced the tip-sample distance by ≈ 20 pm during a constant-height $\Delta f(x,y)$ map (Figure 4a) with a scan speed of 0.25 nm/s. The profiles of the tip-sample stiffness k_{ts} extracted from the $\Delta f(x,y)$ map before and after the distance reduction are shown in Figure 4b,c, respectively. A clear ~ 3 – 4 N/m increase of the absolute average normal force gradient is observed when the tip-sample distance is reduced. This results from the fact that the tip is

forced toward the less attractive force regime (region II in Figure 2) and is accompanied by an increase of the force gradient oscillation amplitude, as expected in friction experiments when increasing the normal load.

We note that, in contrast to conventional friction measurements, we do not excite and detect lateral and vertical deflections of the cantilever. Hence, we cannot directly measure the lateral or normal force signals. Instead, the piezoelectric excitation and detection of the tuning fork sensor performed perpendicular to the surface allow us to measure the normal force gradient. This accounts for the deviation of the signal shape presented in Figure 3c and more profoundly in Figure 4b,c from the standard sawtooth behavior observed in the lateral force traces usually measured in friction experiments. Naturally, the normal force gradient is greatly affected by the exact conformation of the molecule and its orientation within the tip-sample junction. These, in turn, vary with the lateral displacement of the tip and hence provide information regarding the potential energy landscape for the sliding of the molecule on the surface, as depicted in Figure 3a. A similar approach has previously been used to obtain highly resolved AFM images with a CO-decorated tip²⁷ and during vertical manipulations of large polymeric chains.^{30,38,39}

THEORETICAL MODEL

Generalization of the Prandtl–Tomlinson Model.

To understand the experimentally observed frictional behavior, we performed numerical simulations of the approach–retraction curve and the stick–slip motion of the tip decorated with the functionalized porphyrin molecule. While the latter contains many internal degrees of freedom,^{35,45} we postulate that the dominant factors dictating the mechanical response of the system are the σ -bond linking the dicyanophenyl group facing the copper surface to the porphyrin core and the corresponding bond between the CN group facing the surface and the phenyl ring (marked by black arrows in Figure 5a) that are the most flexible bonds in this structure. Based on this assumption, we propose a generalization of the Prandtl–Tomlinson model that implicitly describes the stretching of the σ -bond lengths as well as reorientations of the meso-(3,5-dicyanophenyl) ring with respect to the porphyrin core and of the CN group with respect

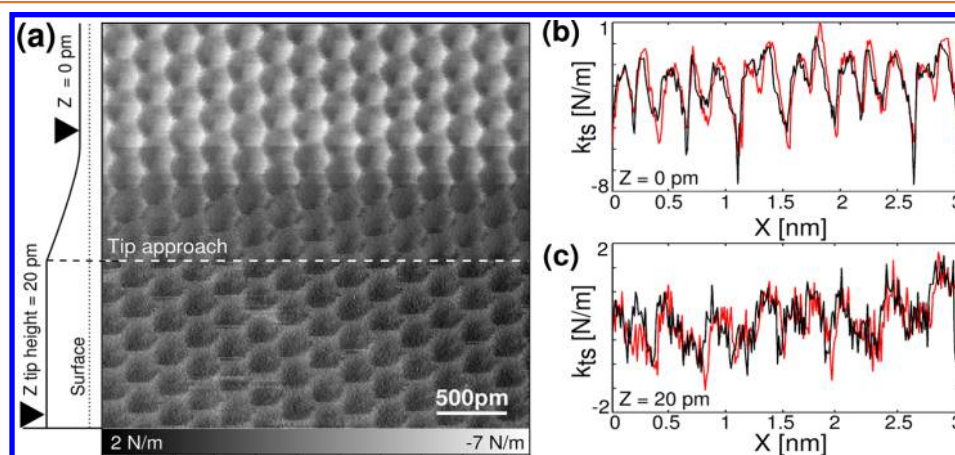


Figure 4. Dependence of the mechanical response during lateral displacement on the tip-sample distance. (a) Tip-sample stiffness map $k_{ts}(x,y)$ obtained with a porphyrin-terminated tip. The scan is from bottom to top; the tip was approached by ≈ 20 pm at the white dashed line while scanning in the region II marked in Figure 2a. (b,c) Typical $k_{ts}(x)$ profiles at tip heights $Z = 0$ and 20 pm, respectively. A significant increase of the absolute mean k_{ts} and an enhancement of the modulation are observed when decreasing the tip-sample distance.

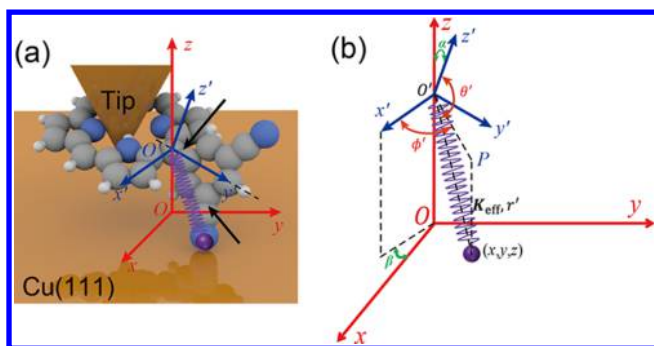


Figure 5. Schematic representation of the model geometry. (a) Definition of the global (x, y, z) and molecular (x', y', z') coordinate systems used in the generalized Prandtl–Tomlinson model. The xy plane of the global system is chosen to be parallel to the surface, whereas the $x'y'$ plane of the molecular system resides at the basal plane of the porphyrin ring. The effective spring connecting the porphyrin ring to the cyano end group interacting with the surface is marked in purple. The noninteracting side groups, e.g., the two *tert*-butyl and one dicyanophenyl end groups, are hidden for clarity purposes. The two black arrows show two σ -bonds that are considered explicitly in DFT calculations. (b) Definition of the porphyrin and effective spring angles. α and β represent the orientation of the molecular coordinate system with respect to the global one. θ' and ϕ' are the orientation angles of the effective spring within the molecular coordinate system. P is the projection of the effective spring vector on the $x'y'$ plane.

to the phenyl side group *via* an effective spring, as depicted in Figure 5. All other internal degrees of freedom of the functionalized molecule and its overall orientation (characterized by the angles α and β in Figure 5b) with respect to the tip remain fixed during the simulation. In order to reduce the parameter space, we chose the Euler angle $\psi = 0$ (angle of rotation around the z' axis), thus ignoring different yawing positions of the molecule with respect to the tip. With this choice, the angles α and β coincide with the remaining Euler angles. The effective spring length and orientation with respect to the molecular coordinate system are defined as r' , θ' , and ϕ' , as shown in Figure 5b. The corresponding stretching (r') and bending (θ' and ϕ') stiffnesses and the equilibrium spring length (r_0') and angles (ϕ_0' and θ_0') required as an input for our model have been obtained *via* DFT calculations. Here, full geometry optimizations of the isolated decorated porphyrin molecule have been performed using the B3LYP⁴⁶ exchange–correlation density functional approximation and the split-valence double- ζ polarized 6-31G** basis set⁴⁷ as implemented in the Gaussian suite of programs.⁴⁸ These were followed by single-point calculations of the stretching and compression of the C–C bond connecting the porphyrin ring to the 3,5-dicyanophenyl unit and the relevant cyano group to its phenyl ring, as well as bending and rotation of these side groups with respect to the corresponding bond axes. The resulting stretching and bending rigidities of the effective spring are presented in Table 1 (see Supporting Information for further details regarding the definition of the effective spring model and

Table 1. Effective Spring Model Parameters Found Based on the DFT Calculations

stiffness (N/m)			equilibrium geometry parameters		
K_r	$K_\theta/r_0'^2$	$K_\phi/r_0'^2$	r_0' (nm)	θ_0' (deg)	ϕ_0' (deg)
27.6	0.623	3.35	0.598	90	54.9

its parametrization). For simplicity, in the following simulations, we ignore anharmonic effects.

As we noted above, we assume that the molecule interacts with the copper surface through a single CN end group. We note, however, that in some configurations both cyano groups may face the surface. In such cases, if one group interacts more strongly with the surface than the other, our model assumptions remain valid, whereas if both groups strongly interact with the surface, the effective spring introduced in the model should be stiffened. We have verified that our results are robust against such stiffening. The CN–surface interaction is modeled using the Steele potential,⁴⁹ originally proposed to describe the physisorption of gases at crystalline surfaces, acting on the free end of the effective spring. The overall interaction potential, U_{ms} , between the molecule and the surface can be written as (in eV units):

$$U_{\text{ms}}(x, y, z) = E_{\text{elastic}} + E_0(z^*) + \frac{U_0 b_s}{2} e^{-a_s(z^* - z_s^*)} U_{xy} \quad (1)$$

with

$$E_{\text{elastic}} = \frac{1}{2} K_r (r' - r_0')^2 + \frac{1}{2} K_\theta (\theta' - \theta_0')^2 + \frac{1}{2} K_\phi (\phi' - \phi_0')^2 \quad (2)$$

$$E_0(z^*) = \frac{2\pi\epsilon_{\text{gs}}A^6}{a_s^*} \left[\frac{2A^6}{5z^{*10}} - \frac{1}{z^{*4}} - \frac{1}{\sqrt{6}(z^* + 0.61\sqrt{2/3})} \right] \quad (3)$$

$$U_{xy} = 2 \cos \frac{2\pi x}{a} \cos \frac{2\pi y}{\sqrt{3}a} + \cos \frac{4\pi y}{\sqrt{3}a} \quad (4)$$

The first term, E_{elastic} , corresponds to the elastic potential of the molecule related to the stretching and bending stiffnesses calculated from DFT (see values in Table 1). The second term, $E_0(z^*)$, describes the distance dependence of the xy potential perpendicular to the surface, where $z^* = z/a$ is the scaled vertical coordinate, with $a = 0.256$ nm being the lattice constant of the Cu(111) surface, $a_s^* = A_s/a^2 = \sqrt{3}/2$, where A_s is the area of unit cell at the surface, $A = \sigma_{\text{gs}}/a$, $\sigma_{\text{gs}} = 1.25$ is the assumed effective diameter, $\epsilon_{\text{gs}} = 0.167$ eV the depth of the Lennard-Jones potential between the end group and the Cu(111) surface, $U_0 = 0.5$ eV (unless specified differently) is the amplitude of the potential in lateral direction, $z_s^* = 0.9$, and $a_s = 13.4$ and $b_s = 13.8$ are fitting parameters for the face-centered cubic (111) surface. The third term describes the corrugation of the Cu(111) surface potential. The details of the Steele potential, which provides a qualitative description of the molecule–surface interaction, can be found in ref 49. The coupled equations of motion derived from this potential for the driven tip and orientation and stretching degrees of freedom of the attached molecule sliding on top of the copper surface are presented in detail in the Supporting Information.

Simulation of the Approach–Retraction. We start by using the generalized Prandtl–Tomlinson model presented above for simulating the approach–retraction traces. Figure 6 presents the variation of the normal force on the tip–surface distance (a) and the corresponding distance between the molecular end group and the surface (b) and its lateral position (c) as well as the variations of the internal degrees of freedom

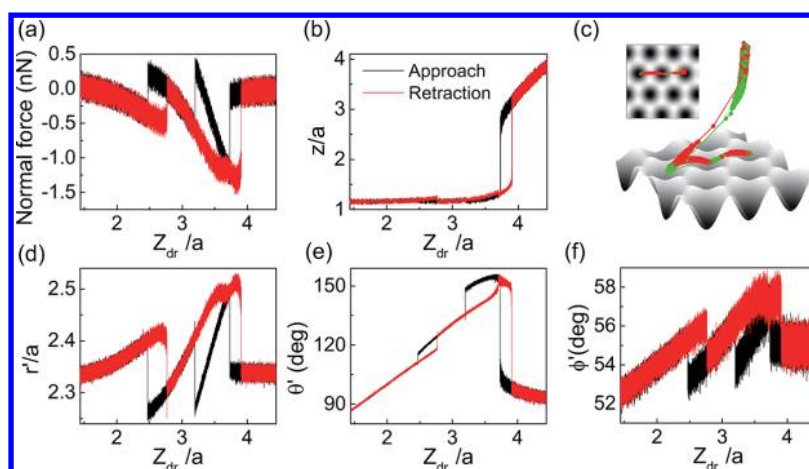


Figure 6. Simulations of approach–retraction cycles. Variations during the approach (black) and retraction (red) traces of the (a) normal force, (b) vertical distance between the end group and the surface, (d) effective spring length, (e,f) rotational angles θ' and ϕ' , respectively. (c) Three-dimensional view of an approach (green)–retraction (red) curve demonstrating the normal and lateral end group displacements during the jumps. Here, $\alpha = 15^\circ$, $\beta = 60^\circ$, $M = 1.0 \times 10^{-12}$ kg, $k_X = k_Y = 6$ N/m, $k_Z = 60$ N/m, $V_{dr} = 0$, $V_{app} = 10$ nm/s, $\gamma_{ms} = \gamma_{mt} = 1.0 \times 10^{-7}$ kg/s, $T = 5$ K (see main text).

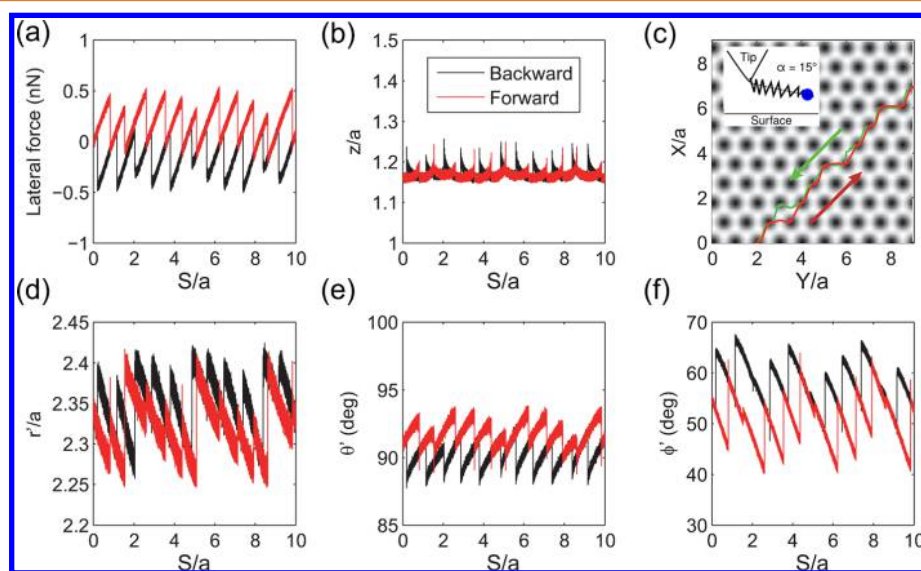


Figure 7. Results of the sliding simulations for $(\alpha, \beta) = (15^\circ, 60^\circ)$. (a) Lateral force as a function of the support displacement. (b) Variation of the distance between the end group of the molecule and the surface. (c) Path of molecular motion along the surface. The red and green arrows mark the tip scanning direction of 45° applied during the forward and backward scans, respectively. (d) Stretching of the molecular bond during sliding. (e,f) Variation of molecular angles during sliding. Other parameters related to the friction simulations (see [Supporting Information](#)) are as follows: $M = 1.0 \times 10^{-12}$ kg, $k_X = k_Y = 6$ N/m, $k_Z = 60$ N/m, $V_{dr} = 25$ nm/s, $\gamma_{ms} = \gamma_{mt} = 1.0 \times 10^{-7}$ kg/s, $T = 5$ K.

of the molecule (d–f). In accordance with the experimental findings, we obtain considerable hysteresis between the approach and retraction force traces. Furthermore, the approach curve demonstrates three abrupt jumps of the normal force, while the retraction counterpart exhibits two such jumps. For both traces, the most distant jump can be identified as a vertical “jump-to/out-of-contact” with the surface associated with the transition from the minima corresponding to the attraction to the tip to that corresponding to the attraction to the surface on the bistable potential (see panel b). Markedly, unlike standard (un)binding transitions, here, the vertical jump is accompanied by a lateral shift of the end group along the surface. This is demonstrated in panel c, showing an approach–retraction trace in three-dimensional view and in panels d–f, where notable variations of the internal degrees of freedom, and, in particular, the rotational angle θ' , are recorded at the

jump position. Importantly, the other end group jumps, which are almost purely lateral, become possible due to the weak stiffness of the rotational degree of freedom θ . This behavior is unique to our setup and results directly from the extra degrees of freedom introduced by the presence of the molecule within the junction. When compared to the experimental results (Figure 2b), the calculated normal force variations during retraction resemble the experimental trace that, as described above, is characterized by two jumps. We note that the number of lateral jumps appearing in our simulations depends on the dissipation constant and hence may reduce from three to two in the approach curve when higher energy dissipation is assumed.

Simulation of Sliding. Figures 7 and 8 show typical results of simulations of friction response obtained for two particular orientations of the porphyrin core with respect to the tip characterized by α and β . Figure 7 corresponds to the

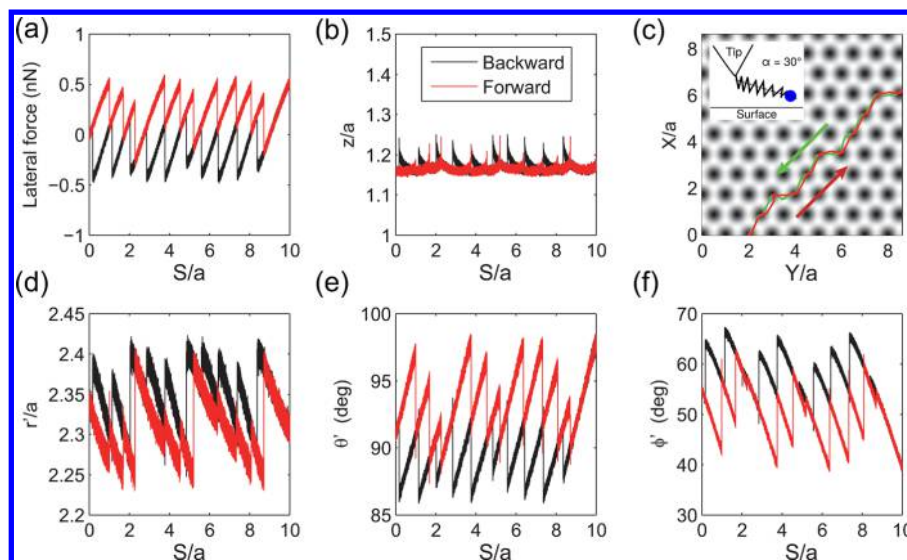


Figure 8. Results of the sliding simulations for $(\alpha, \beta) = (30^\circ, 60^\circ)$; other parameters as well as the panel descriptions are the same as those in Figure 7.

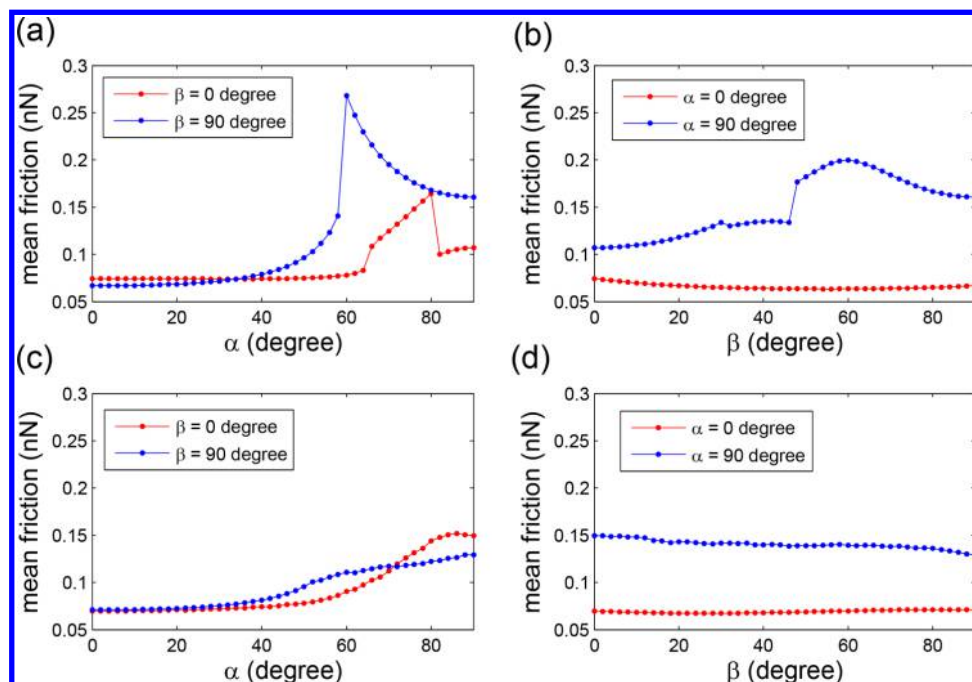


Figure 9. Time-averaged frictional force as a function of the angles α and β characterizing the attachment of the molecule to the tip. (a,c) Dependence on α , (b,d) dependence on β . Parameter values: $M = 1.0 \times 10^{-12}$ kg, $k_X = k_Y = 6$ N/m, $k_Z = 60$ N/m, $U_0 = 0.2$ eV, $V_{dr} = 10$ $\mu\text{m/s}$, $\gamma_{ms} = \gamma_{mt} = 1.0 \times 10^{-7}$ kg/s. In the simulations, the initial distance between the CN group and the surface is set to 0.307 nm. The scan directions are 0° in (a,b) and 45° in (c,d) (see Methods).

porphyrin ring almost parallel to the surface with a mild inclination of 150° , whereas Figure 8 considers its plane inclined by 30° with respect to the surface. To mimic the constant-height maps obtained experimentally, the simulations have been performed by keeping the height of the support constant ($Z_{dr} = 0.524$ nm at $\alpha = 30^\circ$ and 0.434 nm at $\alpha = 15^\circ$) and moving the support in the lateral direction with the constant velocity, $V_{dr} = 25$ nm/s.

Our simulations clearly show (Figures 7a,b and 8a,b) a strong correlation between the stick–slip motion along the lateral direction and dilation of the tip (spring anchor) in the normal direction, thus supporting the general experimental

concept that variations of the normal force gradient can provide information on the frictional response of the system. Noticeably, the vertical response traces (Figures 7b and 8b) considerably deviate from the standard sawtooth pattern of the lateral force (Figures 7a and 8a) in accordance with the experimental observations presented above (Figures 3c and 4b,c). Furthermore, the friction force (calculated from the loop area between lateral force scans (Figures 7a and 8a)) is found to be relatively small with respect to the overall stick–slip oscillation amplitudes. This suggests that the system exhibits nearly superlubric behavior. In both friction traces, stable atomic-scale patterns are obtained due to the single-point

contact formed between the decorated tip and the surface. By comparing the friction force traces of Figure 7a and Figure 8a, we can conclude that the friction forces depend on the orientation of the molecule with respect to the tip characterized by the angles α and β (see Figure 5b). Specifically, the hysteresis loop for the 30°-tilted molecule (Figure 8a) is slightly larger than the one for the 15°-tilted configuration (Figure 7a).

To account for this small difference in the friction force loop between the two considered molecular configurations, we analyze separately the variations of the effective spring length and two orientation angles during the sliding process. Figures 7d and 8d present the variation of the spring length r' for the two tilted ($\alpha = 15^\circ, 30^\circ$) molecular configurations. As can be seen, a very similar dependence of the spring length on the support displacement is found for both molecular configurations. When examining the angle ϕ' , one finds very similar variations in both molecular configurations, as well (Figures 7f and 8f). In contrast, the variations of the angle θ' with support displacement show considerable qualitative and quantitative differences (Figures 7e and 8e). Hence, we can conclude that the difference of friction hysteresis between the 15°- and 30°-tilted molecular configurations originates from the variation of the spring angle θ' . Specifically, with an increase of the molecule tilt angle α , the variations of the spring angle θ' during the sliding process increase.

Finally, to emphasize the importance of the molecular configuration within the tip–surface junction, we present in Figure 9 the dependence of the time-averaged friction force on the angles α and β . We choose two extreme values of 0 and 90° for each of these angles and study the dependence of the time-averaged friction force on the variation of the second angle for two scanning directions. As can be seen in panels a and c of Figure 9, a strong dependence of the friction force on the angle α is obtained. Panels b and d of Figure 9 reveal a much weaker dependence of the frictional force on the angle β . This can be rationalized by the fact that at the perpendicular orientation ($\alpha = 90^\circ$) of the dicyanophenyl leg with respect to the surface the contribution of the bond length variations to the effective lateral frictional forces vanishes and the main contribution comes from the softer degree of freedom of the dicyanophenyl group reorientation. In contrast, in the parallel orientation ($\alpha = 0^\circ$), the main contribution to the effective lateral forces comes from the stiffer bond stretching degree of freedom, while the reorientation contribution is suppressed. Since, according to the Tomlinson model, larger stiffness leads to smaller friction force, we expect to find lower friction the less tilted molecular configuration as found in our simulations. Interestingly, for a scanning direction of 0°, a peak in the mean friction force appears at $(\alpha, \beta) = (66^\circ, 90^\circ)$ and $(80^\circ, 0^\circ)$. This can be attributed to strong fluctuations of the θ' degree of freedom (not shown) which produce additional sliding resistance force. A detailed explanation of this effect can be found in the Supporting Information. Based on our findings, we can conclude that when varying the tip–surface distance, changes of the molecular orientation will modify the contribution of the various internal degrees of freedom to the effective lateral stiffness and hence will affect the overall measured frictional force and contrast as observed in the experiment (see Figure 4).

CONCLUSIONS

To summarize, we have demonstrated that AFM tip decoration by a single porphyrin molecular derivative provides surface imaging with atomic resolution. Furthermore, it is found that

the mechanical response of the internal degrees of freedom of the decorating molecule that depends on its specific configuration within the junction plays a major role in the tribological properties of the system *via* its effect on the stiffness of the forces driving the end group along the surface. Assuming that the molecule interacts with the surface through a single dicyanophenyl side group, we identify the σ -bonds connecting it to the porphyrin core and to the cyano end group as the most important degrees of freedom affecting the measured frictional behavior. This is attributed to the fact that these are the most flexible degrees of freedom within the main backbone of the decorating molecule. To verify this, we have developed a generalized Prandtl–Tomlinson model that describes the dynamic response of these internal molecular degrees of freedom during sliding processes. The microscopic parameters characterizing the relevant stretching and bending rigidities have been extracted from first-principles calculations. Our simulations show that the variation of the normal force gradient during the sliding process is coupled to the lateral frictional forces acting on the CN end group *via* the molecular entity, thus supporting the experimental hypothesis. Furthermore, we have found that external manipulation of the tip, which can result in variations of the molecular configuration, may serve as a control knob to tune the frictional forces and imaging contrast. Our results show that considering the dynamics of the conformational degrees of freedom of the molecule is crucial for understanding the tribological behavior of decorated tips during lateral and vertical manipulations. Hence, systematic investigations of various decorating molecules should provide a better understanding of the impact of the structure and the chemical reactivity of single molecules on their frictional properties at the nanoscale.

METHODS

Scanning Probe Microscopy. Our measurements were realized with a low-temperature STM/AFM microscope (Omicron Nanotechnology GmbH) based on a tuning fork sensor in the qPlus configuration (stiffness of $k = 1800$ N/m, resonance frequency $f_0 = 26$ kHz, Q factor = 35 000) and operated at 5 K in ultrahigh vacuum (UHV). The oscillation amplitudes A_0 employed during the friction experiments were kept below 50 pm. All STM images were recorded in the constant current mode with the bias voltage applied to the tungsten tip. All constant-height Δf maps were conducted with a tip voltage of 300 μ V. Atomically cleaned Cu(111) surfaces were obtained by several cycles of sputtering and annealing under UHV. Molecular depositions were done from a quartz crucible heated to 530 K under UHV on the substrate which was cooled to 80 K in order to avoid spontaneous assemblies.

Generalized Prandtl–Tomlinson model. The generalized Prandtl–Tomlinson model has been simulated by using the Langevin equations; these equations have been propagated using the fourth-order Runge–Kutta method. The algorithm has been implemented in MATLAB. Further details can be found in the Supporting Information. The scan velocity and surface potential amplitude used in the simulations are different from the ones used in the experiments. This is done to reduce computational costs, and we have verified that the general trends remain the same when using the original parametrization.

ASSOCIATED CONTENT

Supporting Information

The Supporting Information is available free of charge on the ACS Publications website at DOI: 10.1021/acsnano.5b05761.

Relaxed coordinates of the isolated porphyrin molecule (XYZ)

Material and methods section as well as the supplementary discussion (PDF)

AUTHOR INFORMATION

Corresponding Authors

*E-mail: remy.pawlak@unibas.ch.

*E-mail: urbakh@post.tau.ac.

*E-mail: ernst.meyer@unibas.ch.

Notes

The authors declare no competing financial interest.

ACKNOWLEDGMENTS

R.P. and E.M. sincerely thank Prof. F. Diederich, Dr. L.-A. Fendt, and Dr. H. Fang for providing the porphyrin derivatives used in this study. R.P., S.K., T.G., A.B., and E.M. acknowledge financial support from the Swiss National Science Foundation (SNSF), the Swiss Nanoscience Institute (SNI), and the COST-Action MP1303. M.U. acknowledges the financial support of the Israel Science Foundation under Grant No. 1316/13. O.H. acknowledges the Lise-Meitner Minerva Center for Computational Quantum Chemistry and the Center for Nanoscience and Nanotechnology at Tel-Aviv University for their generous financial support. W.O. and Q.Z. acknowledge the financial support of the National Key Basic Research Program of China (Grant No. 2013CB934201).

REFERENCES

- (1) Browne, W. R.; Feringa, B. L. Making Molecular Machines Work. *Nat. Nanotechnol.* **2006**, *1*, 25–35.
- (2) Vives, G.; Tour, J. M. Synthesis of Single-Molecule Nanocars. *Acc. Chem. Res.* **2009**, *42*, 473–487.
- (3) Urbakh, M.; Meyer, E. The Renaissance of Friction. *Nat. Mater.* **2010**, *9*, 8–9.
- (4) Socoliuc, A.; Gnecco, E.; Maier, S.; Pfeiffer, O.; Baratoff, A.; Bennewitz, R.; Meyer, E. Atomic-Scale Control of Friction by Actuation of Nanometer-Sized Contacts. *Science* **2006**, *313*, 207–210.
- (5) Maier, S.; Sang, Y.; Filleter, T.; Grant, M.; Bennewitz, R.; Gnecco, E.; Meyer, E. Fluctuations and Jump Dynamics in Atomic Friction. *Phys. Rev. B: Condens. Matter Mater. Phys.* **2005**, *72*, 245418.
- (6) Lantz, M. A.; Wiesmann, D.; Gotsmann, B. Dynamic Superlubricity And The Elimination of Wear at The Nanoscale. *Nat. Nanotechnol.* **2009**, *4*, 586–591.
- (7) Kisiel, M.; Gnecco, E.; Gysin, U.; Marot, L.; Rast, S.; Meyer, E. Suppression of Electronic Friction on Nb Films in The Superconducting State. *Nat. Mater.* **2011**, *10*, 119–122.
- (8) Langer, M.; Kisiel, M.; Pawlak, R.; Pellegrini, F.; Santoro, G. E.; Buzio, R.; Gerbi, A.; Balakrishnan, G.; Baratoff, A.; Tosatti, E.; et al. Giant Frictional Dissipation Peaks and Charge-Density-Wave Slips at The NbSe₂ Surface. *Nat. Mater.* **2014**, *13*, 173–177.
- (9) Kisiel, M.; Pellegrini, F.; Santoro, G.; Samadashvili, M.; Pawlak, R.; Benassi, A.; Gysin, U.; Buzio, R.; Gerbi, A.; Meyer, E.; et al. Non-Contact Dissipation Reveals the Central Peak in SrTiO₃ Phase Transition. *Phys. Rev. Lett.* **2015**, *115*, 046101.
- (10) Mate, C. M.; McClelland, G. M.; Erlandsson, R.; Chiang, S. Atomic-Scale Friction of a Tunneling Tip on a Graphite Surface. *Phys. Rev. Lett.* **1987**, *59*, 1942–1945.
- (11) Bennewitz, R.; Gyalog, T.; Guggisberg, M.; Bammerlin, M.; Meyer, E.; Güntherodt, H.-J. Atomic-Scale Stick-Slip Processes on Cu(111). *Phys. Rev. B: Condens. Matter Mater. Phys.* **1999**, *60*, R11301–R11304.
- (12) Filleter, T.; Paul, W.; Bennewitz, R. Atomic Structure and Friction of Ultrathin Films of KBr on Cu(100). *Phys. Rev. B: Condens. Matter Mater. Phys.* **2008**, *77*, 035430.
- (13) Goryl, M.; Budzioch, J.; Krok, F.; Wojtaszek, M.; Kolmer, M.; Walczak, L.; Konior, J.; Gnecco, E.; Szymonski, M. Probing Atomic-Scale Friction on Reconstructed Surfaces of Single-Crystal Semiconductors. *Phys. Rev. B: Condens. Matter Mater. Phys.* **2012**, *85*, 085308.
- (14) Maier, S.; Gnecco, E.; Baratoff, A.; Bennewitz, R.; Meyer, E. Atomic-Scale Friction Modulated By a Buried Interface: Combined Atomic and Friction Force Microscopy Experiments. *Phys. Rev. B: Condens. Matter Mater. Phys.* **2008**, *78*, 045432.
- (15) Sheehan, P. E.; Lieber, C. M. Nanotribology and Nanofabrication of MoO₃ Structures by Atomic Force Microscopy. *Science* **1996**, *272*, 1158.
- (16) Dietzel, D.; Ritter, C.; Mönninghoff, T.; Fuchs, H.; Schirmeisen, A.; Schwarz, U. D. Frictional Duality Observed During Nanoparticle Sliding. *Phys. Rev. Lett.* **2008**, *101*, 125505.
- (17) Dietzel, D.; Feldmann, M.; Fuchs, H.; Schwarz, U. D.; Schirmeisen, A. Transition From Static to Kinetic Friction of Metallic Nanoparticles. *Appl. Phys. Lett.* **2009**, *95*, 053104.
- (18) Meyer, E.; Overney, R.; Lüthi, R.; Brodbeck, D.; Howald, L.; Frommer, J.; Güntherodt, H.-J.; Wolter, O.; Fujihira, M.; Takano, H.; et al. Friction Force Microscopy of Mixed Langmuir-Blodgett Films. *Thin Solid Films* **1992**, *220*, 132–137.
- (19) Lüthi, R.; Meyer, E.; Haefke, H.; Howald, L.; Gutmannsbauer, W.; Güntherodt, H. J. Sled-Type Motion on The Nanometer Scale: Determination of Dissipation And Cohesive Energies of C₆₀. *Science* **1994**, *266*, 1979–1981.
- (20) Liley, M.; Gourdon, D.; Stamou, D.; Meseth, U.; Fischer, T. M.; Lantz, C.; Stahlberg, H.; Vogel, H.; Burnham, N. A.; Duschl, C. Friction Anisotropy And Asymmetry of a Compliant Monolayer Induced By a Small Molecular Tilt. *Science* **1998**, *280*, 273–275.
- (21) Burns, A. R.; Houston, J. E.; Carpick, R. W.; Michalske, T. A. Friction and Molecular Deformation in the Tensile Regime. *Phys. Rev. Lett.* **1999**, *82*, 1181–1184.
- (22) Frisbie, C. D.; Rozsnyai, L. F.; Noy, A.; Wrighton, M. S.; Lieber, C. M. Functional Group Imaging By Chemical Force Microscopy. *Science* **1994**, *265*, 2071–2074.
- (23) Ito, T.; Namba, M.; Bühlmann, P.; Umezawa, Y. Modification of Silicon Nitride Tips With Trichlorosilane Self-Assembled Monolayers (SAMs) for Chemical Force Microscopy. *Langmuir* **1997**, *13*, 4323–4332.
- (24) Tsukruk, V. V.; Bliznyuk, V. N. Adhesive and Friction Forces Between Chemically Modified Silicon and Silicon Nitride Surfaces. *Langmuir* **1998**, *14*, 446–455.
- (25) Fessler, G.; Zimmermann, I.; Glatzel, T.; Gnecco, E.; Steiner, P.; Roth, R.; Keene, T. D.; Liu, S.-X.; Decurtins, S.; Meyer, E. Orientation Dependent Molecular Friction on Organic Layer Compound Crystals. *Appl. Phys. Lett.* **2011**, *98*, 083119.
- (26) Bartels, L.; Meyer, G.; Rieder, K.-H. Controlled Vertical Manipulation of Single CO Molecule With The Scanning Tunneling Microscope: A Route to Chemical Contrast. *Appl. Phys. Lett.* **1997**, *71*, 213.
- (27) Gross, L.; Mohn, F.; Moll, N.; Liljeroth, P.; Meyer, G. The Chemical Structure of a Molecule Resolved by Atomic Force Microscopy. *Science* **2009**, *325*, 1110–1114.
- (28) Tang, H.; Cuberes, M. T.; Joachim, C.; Gimzewski, J. K. Fundamental Considerations in The Manipulation of a Single C₆₀ Molecule on a Surface With an STM. *Surf. Sci.* **1997**, *386*, 115–123.
- (29) Keeling, D. L.; Humphry, M. J.; Fawcett, R. H. J.; Beton, P. H.; Hobbs, C.; Kantorovich, L. Bond Breaking Coupled with Translation in Rolling of Covalently Bound Molecules. *Phys. Rev. Lett.* **2005**, *94*, 146104.
- (30) Fournier, N.; Wagner, C.; Weiss, C.; Temirov, R.; Tautz, F. S. Force-Controlled Lifting of Molecular Wires. *Phys. Rev. B: Condens. Matter Mater. Phys.* **2011**, *84*, 035435.
- (31) Grill, L.; Rieder, K.-H.; Moresco, F. Exploring The Interatomic Forces Between a Tip and Single Molecules During STM Manipulation. *Nano Lett.* **2006**, *6*, 2685–2689.
- (32) Loppacher, C.; Guggisberg, M.; Pfeiffer, O.; Meyer, E.; Bammerlin, M.; Lüthi, R.; Schlittler, R.; Gimzewski, J. K.; Tang, H.; Joachim, C. Direct Determination of the Energy Required to Operate a Single Molecule Switch. *Phys. Rev. Lett.* **2003**, *90*, 066107.

- (33) Pawlak, R.; Kawai, S.; Fremy, S.; Glatzel, T.; Meyer, E. Atomic-Scale Mechanical Properties of Orientated C₆₀ Molecules Revealed by nc-AFM. *ACS Nano* **2011**, *5*, 6349–6354.
- (34) Pawlak, R.; Kawai, S.; Fremy, S.; Glatzel, T.; Meyer, E. High-Resolution Imaging of C₆₀ Molecules Using Tuning-Fork-Based Non-Contact Atomic Force Microscopy. *J. Phys.: Condens. Matter* **2012**, *24*, 084005.
- (35) Pawlak, R.; Fremy, S.; Kawai, S.; Glatzel, T.; Fang, H.; Fendt, L.-A.; Diederich, F.; Meyer, E. Directed Rotations of Single Porphyrin Molecules Controlled by Localized Force Spectroscopy. *ACS Nano* **2012**, *6*, 6318–6324.
- (36) Hauptmann, N.; Mohn, F.; Gross, L.; Meyer, G.; Frederiksen, T.; Berndt, R. Force and Conductance During Contact Formation to a C₆₀ Molecule. *New J. Phys.* **2012**, *14*, 073032.
- (37) Langewisch, G.; Falter, J.; Fuchs, H.; Schirmeisen, A. Forces During the Controlled Displacement of Organic Molecules. *Phys. Rev. Lett.* **2013**, *110*, 036101.
- (38) Kawai, S.; Koch, M.; Gnecco, E.; Sadeghi, A.; Pawlak, R.; Glatzel, T.; Schwarz, J.; Goedecker, S.; Hecht, S.; Baratoff, A.; et al. Quantifying The Atomic-Level Mechanics of Single Long Physisorbed Molecular Chains. *Proc. Natl. Acad. Sci. U. S. A.* **2014**, *111*, 3968–3972.
- (39) Wagner, C.; Fournier, N.; Tautz, F. S.; Temirov, R. The Role of Surface Corrugation And Tip Oscillation in Single-Molecule Manipulation With Non-Contact Atomic Force Microscope. *Beilstein J. Nanotechnol.* **2014**, *5*, 202–209.
- (40) Fendt, L.-A.; Fang, H.; Zhang, S.; Cheng, F.; Braun, C.; Echegoyen, L.; Diederich, F. Meso,Meso-Linked and Triply Fused Diporphyrins With Mixed-Metal Ions: Synthesis and Electrochemical Investigations. *Eur. J. Org. Chem.* **2007**, *2007*, 4659–4673.
- (41) Lafferentz, L.; Ample, F.; Yu, H.; Hecht, S.; Joachim, C.; Grill, L. Conductance of a Single Conjugated Polymer as a Continuous Function of Its Length. *Science* **2009**, *323*, 1193–1197.
- (42) Such, B.; Glatzel, T.; Kawai, S.; Meyer, E.; Turanský, R.; Brndiar, J.; Stich, I. Interplay of The Tip-Sample Junction Stability and Image Contrast Reversal on a Cu(111) Surface Revealed by The 3D Force Field. *Nanotechnology* **2012**, *23*, 045705–7.
- (43) Nakanishi, S.; Horiguchi, T. Surface Lattice Constant of Si(111), Ni(111) and Cu(111). *Jpn. Journ. Appl. Physics* **1981**, *20*, L214–L216.
- (44) König, T.; Simon, G. H.; Rust, H.-P.; Heyde, M. Atomic Resolution on a Metal Single Crystal With Dynamic Force Microscopy. *Appl. Phys. Lett.* **2009**, *95*, 083116.
- (45) Boukari, K.; Sonnet, P.; Duverger, E. DFT-D Studies of Single Porphyrin Molecule on Doped Boron Silicon Surfaces. *ChemPhysChem* **2012**, *13*, 3945–3951.
- (46) Becke, A. D. Density-Functional Thermochemistry. III. The Role of Exact Exchange. *J. Chem. Phys.* **1993**, *98*, 5648–5652.
- (47) Hariharan, P. C.; Pople, J. A. The Influence of Polarization Functions on Molecular Orbital Hydrogenation Energies. *Theor. Chem. Acc.* **1973**, *28*, 213–222.
- (48) Frisch, M. J.; Trucks, G. W.; Schlegel, H. B.; Scuseria, G. E.; Robb, M. A.; Cheeseman, J. R.; Scalmani, G.; Barone, V.; Mennucci, B.; Petersson, G. A.; Nakatsuji, H.; et al. *Gaussian 09*, revision A.02; Gaussian, Inc.: Wallingford, CT, 2009.
- (49) Steele, W. A. The Physical Interaction of Gases With Crystalline Solids: I. Gas-Solid Energies And Properties of Isolated Adsorbed Atoms. *Surf. Sci.* **1973**, *36*, 317.